Controlling Rayleigh-Taylor Instabilities in Magnetically Driven Solid Metal Shells by Means of a Dynamic Screw Pinch

P. F. Schmit,[1] A. L. Velikovich,[2] R. D. McBride,[1,3] and G. K. Robertson[1]
[1]Sandia National Laboratories, P. O. Box 5800, Albuquerque, New Mexico 87185-1186, USA
[2]Plasma Physics Division, Naval Research Laboratory, Washington, District of Columbia 20375, USA
[3]Nuclear Engineering and Radiological Sciences, University of Michigan, Ann Arbor, Michigan 48109, USA
(Received 14 June 2016; revised manuscript received 11 October 2016; published 11 November 2016)

Magnetically driven implosions of solid metal shells are an effective vehicle to compress materials to extreme pressures and densities. Rayleigh-Taylor instabilities (RTI) are ubiquitous, yet typically undesired features in all such experiments where solid materials are rapidly accelerated to high velocities. In cylindrical shells ("liners"), the magnetic field driving the implosion can exacerbate the RTI. We suggest an approach to implode solid metal liners enabling a remarkable reduction in the growth of magnetized RTI (MRTI) by employing a magnetic drive with a tilted, dynamic polarization, forming a dynamic screw pinch. Our calculations, based on a self-consistent analytic framework, demonstrate that the cumulative growth of the most deleterious MRTI modes may be reduced by as much as 1 to 2 orders of magnitude. One key application of this technique is to generate increasingly stable, higher-performance implosions of solid metal liners to achieve fusion [M. R. Gomez *et al.*, Phys. Rev. Lett. **113**, 155003 (2014)]. We weigh the potentially dramatic benefits of the solid liner dynamic screw pinch against the experimental tradeoffs required to achieve the desired drive field history and identify promising designs for future experimental and computational studies.

DOI: 10.1103/PhysRevLett.117.205001

In this Letter, we describe a novel approach to suppress the growth of detrimental Rayleigh-Taylor instabilities (RTI) [1,2] in rapidly imploding, cylindrical metal shells ("liners"). In high energy density (HED) and inertial confinement fusion (ICF) research, RTI are pervasive and usually undesired. Enabled by the world's leading pulsed-power facilities, including the 26 MA, 80 TW "Z" Facility at Sandia National Laboratories [3], magnetically driven implosions of solid liners are an efficient approach to study HED [4] and ICF [5–7] physics. However, such implosions require multi-Mbar pressures surpassing the yield strength of the initially solid targets, resulting in accelerating, convergent shells of electrically conducting fluid subject to magnetically enhanced RTI (MRTI) [8].

The severity of MRTI necessitates the use of initially thick, massive liners to maintain the shell's integrity in flight [4,5]. Reducing MRTI growth could enable the use of thinner (and possibly higher-density) liners, increasing achievable peak shell velocities, shell ram pressures, fuel stagnation pressures, and/or fuel confinement times. Extensive experimental and computational work has examined the formation [9–12] and evolution [5,13–18] of MRTI in metal liners. Several authors also examine RTI in cylindrical shells analytically [8,19–24]. Specifically, Velikovich and Schmit (VS) [24] describe MRTI in thick shells composed of ideal fluid. VS asymptotically recovers the behavior of MRTI in various limits described in previous works [8,20,22], while it also includes the so-called "Bell-Plesset effects" [25,26] accounting for the convergent motion of the shell. Importantly, VS provides a self-consistent framework to analyze (linear) MRTI in thick conducting shells.

Given their virulent nature, methods to mitigate RTI abound. In both laser "indirect-drive" [27–32] and "direct-drive" [33–35] spherical capsule implosions, RTI is controlled via ablative stabilization [36–42]. However, stabilizing mass ablation does not occur in magnetically driven liner implosions. In diffuse z pinches, MRTI is controlled by mass accretion [43] or by tailoring the initial density [44,45] or velocity shear [46,47] profiles. Yet, these methods are not easily applicable to the relatively slow implosions of dense metal shells. On the other hand, coating metal liners with an insulator appears to improve liner stability by modifying the electrothermal instability (ETI) [9,10,18] and suppressing early-time density modulations of the liner's outer surface. Like high-Z coatings [48,49] and mid-Z doping [50–52] for direct-drive and adiabat shaping [53] for indirect-drive spherical capsule implosions, ETI mitigation lowers the seed amplitude for MRTI, which later grows exponentially in flight.

Magnetic shear also suppresses MRTI [54]. In pinches, the most deleterious instabilities are interchange modes [8], satisfying $\boldsymbol{\kappa} \cdot \mathbf{B} = 0$. Here, $\boldsymbol{\kappa}$ is the perturbation wave vector, and $\mathbf{B}$ is the magnetic field. Interchange modes rearrange magnetic field lines without bending them, thereby avoiding magnetic tension effects that would otherwise increase the energy cost and slow the growth of perturbations. Sufficient directional shear of $\mathbf{B}$ within magnetized plasma ensures $\boldsymbol{\kappa} \cdot \mathbf{B} \neq 0$ for all $\boldsymbol{\kappa}$, suppressing

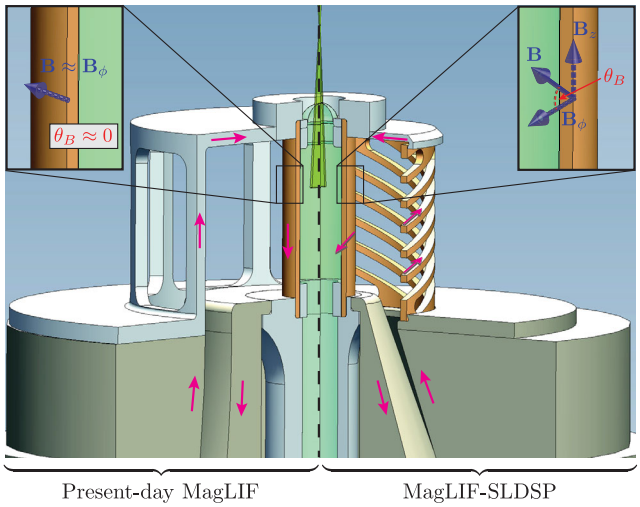

FIG. 1. Example solid liner dynamic screw pinch design for MagLIF, compared to present-day MagLIF. The slotted return current can is replaced with a helically machined can. The direction of current flow is indicated by magenta arrows. Preheat laser enters the target from above. Insets show the drive magnetic field orientation for each target and define the polarization angle, θ_B. (Note: θ_B also includes a contribution from any applied external $\mathbf{B}_z$ field, not shown here.)

interchange modes and enhancing stability. However, for metal liners driven by short [$\mathcal{O}(100$ ns)], intense electrical pulses, the shell thickness Δ typically greatly exceeds the corresponding magnetic skin depth. Thus, most of the drive field remains near the liner's outer surface, precluding the formation of a stabilizing sheared $\mathbf{B}$ profile within the bulk liner material.

To stabilize MRTI in solid liner experiments, we propose redirecting the ambient power flow in a helical direction, whereby dynamic axial and azimuthal field components are generated simultaneously near the liner's outer surface, forming a solid liner dynamic screw pinch (SLDSP). The external drive field generates a stabilizing surface tension at the vacuum-liner interface, $T_{\mathrm{eff}} \approx (\mu_0/2\pi\kappa^3)(\boldsymbol{\kappa}\cdot\mathbf{B})^2$ [19], where $|\boldsymbol{\kappa}| = \kappa$. Nevertheless, the interchange modes ($\boldsymbol{\kappa}\cdot\mathbf{B} = 0$) once again evade stabilization. In z pinches, these are the azimuthally symmetric "sausage" modes [15,16], which satisfy $\boldsymbol{\kappa}\cdot\mathbf{B} = 0$ throughout the implosion. Yet, the helical interchange modes of the SLDSP always develop a field-aligned component (and finite T_{eff}) in flight. The absence of magnetic shear in the SLDSP allows pure interchange modes to exist momentarily, but the apparent rotation of magnetic field lines near the outer surface of the SLDSP preferentially drives a continuously varying spectrum of interchange modes in flight, remarkably reducing the growth of the most damaging modes by as much as $\mathcal{O}(10^1 - 10^2)$.

Figure 1 shows an implementation of this strategy for the magnetized liner inertial fusion (MagLIF) concept [5–7]. Helically twisted return current posts form a solenoid, so the liner sees $\mathbf{B}[r = r_l(t)] = B_\phi(t)\hat{\boldsymbol{\phi}} + B_z(t)\hat{\mathbf{z}} \approx \mu_0 I(t)[(1/2\pi r_l(t))\hat{\boldsymbol{\phi}} + n_c\hat{\mathbf{z}}]$, where I is the liner axial current, r_l is the liner's unperturbed outer radius, and n_c is the turns-per-unit-length of each post. The polarization of $\mathbf{B}$ at $r = r_l(t)$ obeys $\theta_B(t) = \tan^{-1}(B_z/B_\phi) = \tan^{-1}[2\pi n_c r_l(t)]$, rotating toward the equatorial plane of the liner during the implosion. The perturbation wave vector, $\boldsymbol{\kappa} = (m/r_l)\hat{\boldsymbol{\phi}} + (2\pi k/L)\hat{\mathbf{z}}$, also rotates toward the equatorial plane and increases in magnitude during the implosion when $m \neq 0$. Here, L is the axial length of the liner, and k and m are the integer axial and azimuthal mode numbers, respectively. Initially, the most unstable (interchange) modes satisfy $m = -[2\pi r_l(0)]^2 n_c k/L \neq 0$, but they quickly obtain a field-aligned component and finite T_{eff} in flight according to $d/dr_l(\boldsymbol{\kappa}\cdot\mathbf{B}) = -\mu_0 mI/\pi r_l^3$.

Dynamic B_z generation in thin foil [12], gas puff [55,56], and wire array [57] experiments demonstrated qualitative impacts on stability. However, detailed analyses of these experiments are lacking, and our understanding of MRTI in these complex systems is either cursory [58,59] or nonexistent. Furthermore, no enhancement of x-ray or neutron production was observed in these systems. For each of these experiments, significant drive magnetic field penetration into the target is possible (and often measured [12,57]), invalidating a simple ideal MHD picture and suggesting that magnetic shear may play a role, but this remains an open question. In stark contrast, thick metal liners are much more amenable to an ideal MHD treatment like VS, and the dominant physics influencing the MRTI—including the dynamic-polarization stabilization exhibited by the SLDSP—is less ambiguous. Also, unlike other pinches utilizing helical currents [55–57], the SLDSP could significantly enhance the performance of magnetic direct drive ICF experiments.

We demonstrate the remarkable stabilizing effect of the SLDSP using the self-consistent VS model for linear MRTI in thick, magnetically driven cylindrical shells of incompressible, perfectly conducting fluid [24]. We choose the initial outer radius $r_l(0) \equiv r_{l0} = 2.79$ mm, initial aspect ratio $AR = r_{l0}/\Delta = 24$, and shell mass density $\rho = 6930$ kg/m^3, such that r_{l0} and the line mass density resemble present-day MagLIF experiments using thick ($AR = 6$) beryllium liners [7]. The $AR = 24$ incompressible shell maintains a similar $r_l(t)$ history as the thicker, compressible MagLIF liners, improving surrogacy with present-day experiments. Figure 2(a) shows the liner trajectory and drive pressure history for the "null" case with straight return current posts, calculated using a realistic circuit model for Z [60]. Like MagLIF, an initial axial field $B_z = 10$ T exists outside and inside the shell, but here its only dynamical significance is to facilitate stagnation via a brief ($\approx$1 ns) surge in magnetic backpressure at the liner's inner surface, $r = r_g(t)$, due to flux compression [61]. During the acceleration-MRTI phase, B_z is too weak to provide any shear stabilization.

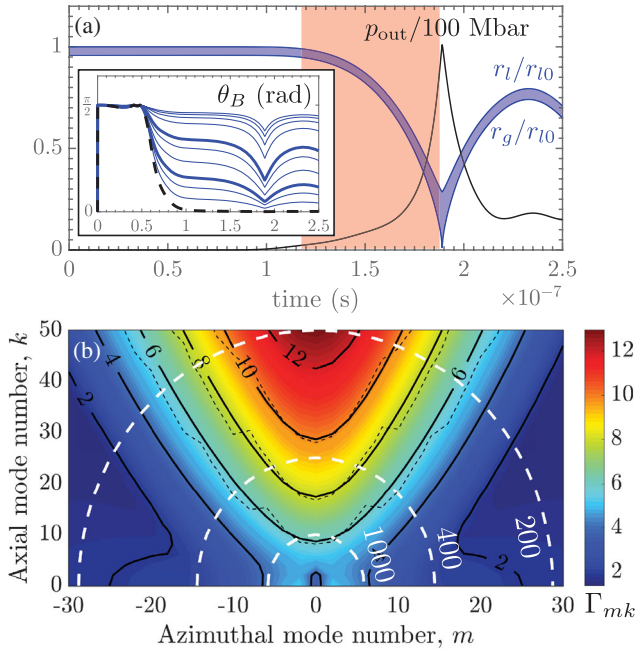

FIG. 2. (a) $AR = 24$ incompressible liner trajectory (blue fill) and magnetic pressure history at liner's outer surface, p_{out}. Red shading shows MRTI calculation interval. Inset: magnetic field polarization angle, $\theta_B(t) = \tan^{-1}(B_z/B_\phi)$, near the liner's outer (unstable) surface for several SLDSP scenarios. Dashed black line is the null case, $n_c \to 0$ and initial $B_z = 10$ T. (b) Spectrum of MRTI e-foldings, Γ_{mk}, for the null case. Dashed black lines show exact solutions $\Gamma_{exact} \in \{6, 8, 10\}$. Dashed white lines indicate $\lambda(t_2)$, i.e., the MRTI mode wavelength (in μm) at the end of the MRTI calculation.

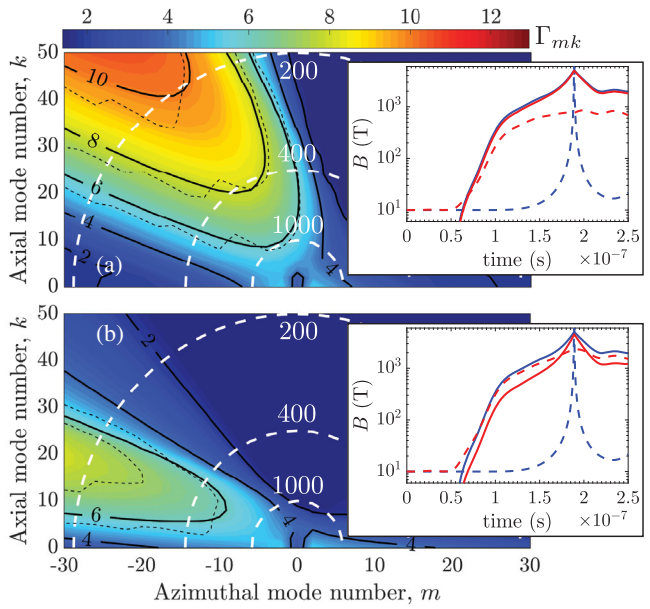

FIG. 3. Spectra of MRTI e-foldings, Γ_{mk}, for liner trajectory and drive pressure history shown in Fig. 2(a), but with (a) $n_c L = 0.33$ and (b) $n_c L = 1.0$. Lower and upper thick, solid lines in Fig. 2(a) inset show θ_B for (a) and (b), respectively. Dashed black lines show exact solutions $\Gamma_{exact} \in \{6, 8, 10\}$. Dashed white lines indicate $\lambda(t_2)$, i.e., the MRTI mode wavelength (in μm) at the end of the MRTI calculation. Insets: B_ϕ (solid, red) and B_z (dashed, red) at $r = r_l(t)$ of SLDSP relative to B_ϕ for the null case (solid, blue) and the flux-compressed B_z inside the liner (dashed, blue).

Figure 2(b) shows the MRTI e-folding spectrum, $\Gamma_{mk} = \int_{t_1}^{t_2} \gamma_{mk}(t')dt'$, for the null case, $n_c = 0$. Note, perturbation quantities grow as $\xi(t_2) \approx \xi(t_1) \exp \Gamma_{mk}$. The time interval $[t_1, t_2]$ signifies the main acceleration-MRTI phase, from the time the liner undergoes 1% relative displacement (t_1) to a "mixed" deceleration onset time (t_2), halfway between the onset of deceleration of the liner's inner and outer surfaces. Here, γ_{mk} is the VS instantaneous exponential growth rate for mode numbers (m, k). Supplemental Material containing the formulas used to compute γ_{mk} accompanies this Letter [62]. We also show contours of the exact solutions $\Gamma_{exact} \in \{6, 8, 10\}$ [63], suggesting that our use of an instantaneous, exponential growth rate is reasonable. As expected, the $m = 0$ sausage modes are the most unstable [8].

We examine the stability of the SLDSP by varying n_c while maintaining the same pressure history, $p_{out}(t) = (B_\phi^2 + B_z^2)_{r=r_l}/(2\mu_0)$, and liner trajectory as the null case in Fig. 2(a). The inset in Fig. 2(a) shows $\theta_B(t)$ for several SLDSP scenarios, where $n_c L \in [0.2, 10]$. Figures 3(a) and 3(b) show Γ_{mk} for the cases $n_c L = 0.33$ and 1.0, respectively. Early in time, $B_z \gtrsim B_\phi$, with B_z rapidly exceeding 100 T before MRTI commences and peaking at $\mathcal{O}(1000$ T). Here, $\theta_B(t_1) \gtrsim \pi/4$, and the interchange modes ($\boldsymbol{\kappa} \cdot \mathbf{B} = 0$) are initially helical $(m, k \neq 0)$. Yet, B_ϕ always becomes dominant, so $d\theta_B/dt < 0$, and these modes quickly generate field-oriented components in flight. Figures 3(a) and 3(b) both show reduced MRTI growth compared to the null case, Fig. 2(b), and Fig. 3(b) represents a near-optimum among the cases considered here. When $n_c L \gg 1$ (the θ-pinch limit), the $k = 0$ "flute" modes exceed the growth of the helical MRTI. Note from the Fig. 3 insets that the flux-compressed B_z inside the liner is $\ll B_\phi$ for most of the implosion, so shear stabilization is absent.

The SLDSP reduces $\Gamma_{200} \equiv \max(\{\Gamma_{mk} : \lambda(t_2) = 200\ \mu\text{m}\})$ by as much as $\delta\Gamma_{200} = -5.1$ relative to the null case [64], a 170-fold reduction of the (linear) mode amplitude at this wavelength. $|\delta\Gamma|$ diminishes at longer wavelengths, since the stabilizing surface-tension effect scales like $\mathcal{K}T_{\text{eff}} \propto \kappa^2 T_{\text{eff}} \propto \kappa$, where $\mathcal{K}$ is the perturbed interface curvature [19]. For Fig. 3(b), $\delta\Gamma_{400} = -2.8$ (18 in terms of amplitude) and $\delta\Gamma_{1000} = -1.1$ (3 in terms of amplitude). Hence, the SLDSP reduces acceleration-MRTI growth by $\mathcal{O}(10^1$–$10^2)$ in the $\lambda = \mathcal{O}(\Delta)$ band. Simulations suggest that modes with $\lambda \ll \Delta$ do not contribute substantially to the observed MRTI growth in experiments [15], while modes with $\lambda \gg \Delta$ do not grow quickly enough to impact the implosion quality substantially. Intermediate-wavelength modes balance fast growth with significant "feedthrough," whereby perturbations of the unstable outer

surface during acceleration leave an imprint on the inner surface, smaller in amplitude by roughly $\exp(-\kappa\Delta)$ [8,65]. These inner-surface perturbations destabilize during deceleration, inhibiting the conversion of liner kinetic energy to fuel thermal energy and exacerbating the mix of liner material into the fuel.

In experiments, practical constraints may prevent the realization of some SLDSP solutions. The dynamic B_z generation increases the total load inductance seen by the pulsed power driver, reducing the peak current that can be coupled to the load and potentially exacerbating current losses elsewhere in the system [66–68]. Accordingly, SLDSP designs must balance enhanced liner stability with potentially diminished driver-target coupling. Optimizing a particular design will require some combination of detailed 3D simulations and experimental platform validation, which are beyond the scope of this initial study. Numerical 3D calculations could compliment our theoretical analysis by assessing the importance of finite liner resistivity and compressibility, nonlinear mode saturation, and mode-mode coupling of the MRTI. (Note that unlike other RTI mitigation techniques amenable to 2D analyses, e.g., Refs. [38,41,43,44], the SLDSP is a distinctly 3D object.)

Instead, we show here that a plausible design space exists for one important system—MagLIF [5–7]—where the SLDSP could outperform the present-day experimental platform [7] due to 3D MRTI stabilization. We modified the recently developed Semi-Analytic MagLIF Model (SAMM) [60,69] to consider the SLDSP scenario depicted in Fig. 1. The Z equivalent circuit model (Sec. II-B of Ref. [60]) is augmented so that the dynamic inductance of the liner ($L_v(t) = (\mu_0 L/2\pi)\ln[r_{rc}/r_l(t)]$, where r_{rc} is the radius of the return current posts) is driven in series with an ideal solenoidal circuit element with inductance $L_s(t) = \pi[r_{rc}^2 - r_l^2(t)]\mu_0 L n_c^2$, representing the effect of the twisted posts. To achieve lower inductances, we examine r_{rc} below its nominal value of 13 mm. We also automate the design of power feeds accommodating the reduced r_{rc} as illustrated in Fig. 1, changing the static inductance L_0 in the circuit model [60]. Finally, we estimate additional current losses using a shunt resistor model developed for MagLIF loads [70], which typically restricts peak currents to 17–18 MA in present-day experiments. Driving the circuit with Z's nominal 130-ns open-circuit voltage waveform, a variety of drive pressure histories and compressible liner trajectories can be considered.

Figure 4(a) compares the stability of the SLDSP with present-day MagLIF experiments. To estimate MRTI growth, we use the liner's outer surface dynamics (r_l and its time derivatives) given by SAMM in γ_{mk} and prescribe the time derivatives of $r_g(t)$ assuming the liner is instantaneously incompressible; e.g., $dr_g/dt = (r_l/r_g)dr_l/dt$. Although the analysis is no longer self-consistent, reasonable accuracy is obtained, since the motion of the unstable surface, $r_l(t)$, predominantly sets

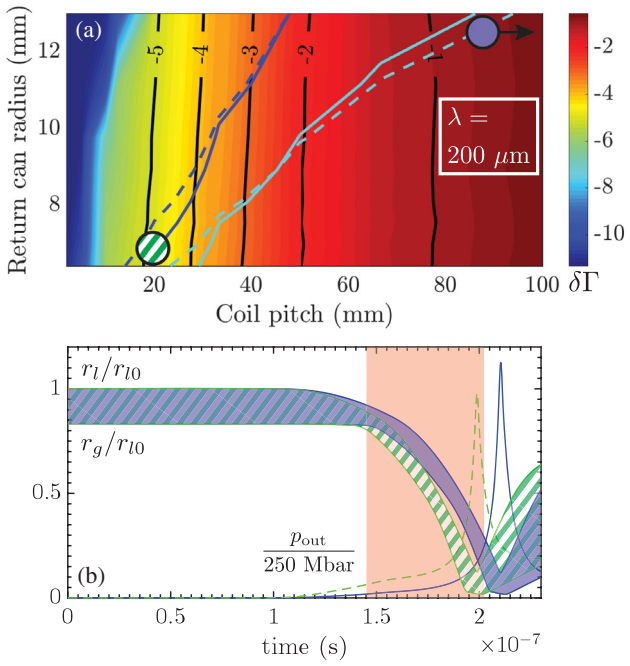

FIG. 4. Evaluation of MagLIF platform stability and performance incorporating SLDSP techniques. (a) MRTI e-folding reduction ($\delta\Gamma$) relative to the null case for $\lambda(t_2) = 200\ \mu$m by varying the return current radius, r_{rc}, and coil pitch, $d = 1/n_c$. Rightmost solid and dashed lines (cyan) are, respectively, the thresholds for ≤ 8 nH initial load inductance and 1D neutron yields $\geq 90\%$ relative to the null case. Leftmost solid and dashed lines (blue) assume a 2 nH load-inductance reduction by other means. (Note: $d \to \infty$ in the null case.) (b) $AR = 6$ beryllium liner trajectory (solid fill) and drive pressure history (solid line) representing present-day MagLIF (null case), and trajectory (hatched fill) and pressure history (dashed line) for SLDSP with $n_c L = 0.5$ and 2 nH load-inductance reduction, corresponding approximately to the target geometries shown in Fig. 1. Red shading indicates MRTI calculation interval for null case. Filled circles in (a) correspond to parameters for similarly filled trajectories in (b).

γ_{mk} during acceleration MRTI. To help identify promising SLDSP designs, we plot the thresholds for similar 1D fusion yields ($\geq 90\%$, according to SAMM) and load inductances (≤ 8 nH) relative to present-day experiments. Yields are a sensible surrogate for the total work done on the preheated fuel, while the inductance threshold represents an approximate limit where we expect our current loss models to be predictive. Ongoing efforts suggest that load inductance reductions of 2–3 nH are achievable through improved hardware design, so we also plot these thresholds assuming an additional 2 nH reduction by other means, allowing for more aggressive SLDSP designs (i.e., greater $n_c L$) satisfying the maximum 8 nH load-inductance constraint. Promising design parameters are found to the right of these curves in Fig. 4(a).

Subject to these yield and inductance constraints, Fig. 4(a) shows $|\delta\Gamma_{200}| \lesssim 5$, while $|\delta\Gamma_{400}| \lesssim 3$ (not shown), so the growth of the $\lambda = \mathcal{O}(\Delta)$ modes is once again reduced

by $\mathcal{O}(10^1$–$10^2)$. Optimal designs favor minimizing r_{rc} and only modest turning of the return current posts over the height of the liner ($n_c L < 1$). Figure 4(b) compares the calculated liner trajectories and drive pressure histories of a present-day MagLIF experiment with a promising SLDSP solution, corresponding approximately to the two configurations shown in Fig. 1. Although the peak drive pressure of the SLDSP is slightly lower than the null case, stagnation occurs almost 10 ns earlier. Both cases have similar initial load inductance and early-time load current histories (until $t \approx 1.6 \times 10^{-7}$ s), yet the dynamic B_z generated by the SLDSP increases the drive pressure by $[1 + (2\pi r_l n_c)^2]$ for a given load current, leading to faster early acceleration of the liner. Although an analysis of other perturbing mechanisms like the electrothermal instability [9,10,18] is not included here, the steeper initial dp_{out}/dt may provide less time for instabilities like ETI to develop [9], further enhancing stability.

By tuning the polarization of the magnetic drive, the solid liner dynamic screw pinch (SLDSP) offers a new pathway to enhance the implosion stability of thick metal liners dramatically, enabling higher-performance magnetically driven implosions for high energy density and inertial confinement fusion research. The SLDSP magnetically stabilizes the most deleterious Rayleigh-Taylor instability modes in flight, potentially reducing their cumulative growth by $\mathcal{O}(10^1$–$10^2)$. Analysis of the tradeoffs between enhanced stability and diminished current delivery in experiments points toward an immediate application space on drivers like Z.

The authors gratefully acknowledge Adam Sefkow, Matthew Martin, Kyle Peterson, Matthew Weis, Mike Desjarlais, and Dan Sinars for helpful discussions. We also are grateful to the referees for helpful suggestions regarding the manuscript. This research was supported in part by an appointment to the Sandia National Laboratories Truman Fellowship in National Security Science and Engineering, which is part of the Laboratory Directed Research and Development (LDRD) Program, Project No. 165746, and sponsored by Sandia Corporation (a wholly owned subsidiary of Lockheed Martin Corporation) as Operator of Sandia National Laboratories under its U.S. Department of Energy Contract No. DE-AC04-94AL85000.

[1] L. Rayleigh, Proc. London Math. Soc. **14**, 170 (1883).
[2] G. Taylor, Proc. R. Soc. A **201**, 192 (1950).
[3] M. E. Cuneo *et al.*, IEEE Trans. Plasma Sci. **40**, 3222 (2012).
[4] R. W. Lemke *et al.*, J. Appl. Phys. **119**, 015904 (2016).
[5] S. A. Slutz, M. C. Herrmann, R. A. Vesey, A. B. Sefkow, D. B. Sinars, D. C. Rovang, K. J. Peterson, and M. E. Cuneo, Phys. Plasmas **17**, 056303 (2010).
[6] A. B. Sefkow, S. A. Slutz, J. M. Koning, M. M. Marinak, K. J. Peterson, D. B. Sinars, and R. A. Vesey, Phys. Plasmas **21**, 072711 (2014).
[7] M. R. Gomez *et al.*, Phys. Rev. Lett. **113**, 155003 (2014).
[8] E. G. Harris, Phys. Fluids **5**, 1057 (1962).
[9] K. J. Peterson, D. B. Sinars, E. P. Yu, M. C. Herrmann, M. E. Cuneo, S. A. Slutz, I. C. Smith, B. W. Atherton, M. D. Knudson, and C. Nakhleh, Phys. Plasmas **19**, 092701 (2012).
[10] K. J. Peterson, T. J. Awe, E. P. Yu, D. B. Sinars, E. S. Field, M. E. Cuneo, M. C. Herrmann, M. Savage, D. Schroen, K. Tomlinson, and C. Nakhleh, Phys. Rev. Lett. **112**, 135002 (2014).
[11] J.-K. Dan, X.-D. Ren, X.-B. Huang, K. Ouyang, and G.-H. Chen, Phys. Plasmas **21**, 122711 (2014).
[12] L. Atoyan, D. A. Hammer, B. R. Kusse, T. Byvank, A. D. Cahill, J. B. Greenly, S. A. Pikuz, and T. A. Shelkovenko, Phys. Plasmas **23**, 022708 (2016).
[13] D. B. Sinars *et al.*, Phys. Rev. Lett. **105**, 185001 (2010).
[14] D. B. Sinars *et al.*, Phys. Plasmas **18**, 056301 (2011).
[15] R. D. McBride *et al.*, Phys. Rev. Lett. **109**, 135004 (2012).
[16] R. D. McBride *et al.*, Phys. Plasmas **20**, 056309 (2013).
[17] T. J. Awe *et al.*, Phys. Rev. Lett. **111**, 235005 (2013).
[18] T. J. Awe, K. J. Peterson, E. P. Yu, R. D. McBride, D. B. Sinars, M. R. Gomez, C. A. Jennings, M. R. Martin, S. E. Rosenthal, D. G. Schroen, A. B. Sefkow, S. A. Slutz, K. Tomlinson, and R. A. Vesey, Phys. Rev. Lett. **116**, 065001 (2016).
[19] S. Chandrasekhar, *Hydrodynamic and Hydromagnetic Stability* (Clarendon Press, Oxford, 1961), Chap. X.
[20] A. B. Bud'ko, F. S. Felber, A. I. Kleev, M. A. Liberman, and A. L. Velikovich, Phys. Fluids B **1**, 598 (1989).
[21] O. A. Hurricane, Phys. Fluids **17**, 058103 (2005).
[22] D. D. Ryutov and M. A. Dorf, Phys. Plasmas **21**, 112704 (2014).
[23] M. R. Weis, P. Zhang, Y. Y. Lau, P. F. Schmit, K. J. Peterson, M. Hess, and R. M. Gilgenbach, Phys. Plasmas **22**, 032706 (2015).
[24] A. L. Velikovich and P. F. Schmit, Phys. Plasmas **22**, 122711 (2015).
[25] G. I. Bell, Los Alamos Scientific Laboratory Report No. LA-1321, 1951.
[26] M. S. Plesset, J. Appl. Phys. **25**, 96 (1954).
[27] M. M. Marinak, S. G. Glendinning, R. J. Wallace, B. A. Remington, K. S. Budil, S. W. Haan, R. E. Tipton, and J. D. Kilkenny, Phys. Rev. Lett. **80**, 4426 (1998).
[28] M. M. Marinak, S. W. Haan, T. R. Dittrich, R. E. Tipton, and G. B. Zimmerman, Phys. Plasmas **5**, 1125 (1998).
[29] T. R. Dittrich, O. A. Hurricane, D. A. Callahan, E. L. Dewald, T. Döppner, D. E. Hinkel, L. F. Berzak Hopkins, S. Le Pape, T. Ma, J. L. Milovich, J. C. Moreno, P. K. Patel, H.-S. Park, B. A. Remington, J. D. Salmonson, and J. L. Kline, Phys. Rev. Lett. **112**, 055002 (2014).
[30] V. A. Smalyuk, D. T. Casey, D. S. Clark, M. J. Edwards, S. W. Haan, A. Hamza, D. E. Hoover, W. W. Hsing, O. Hurricane, J. D. Kilkenny, J. Kroll, O. L. Landen, A. Moore, A. Nikroo, L. Peterson, K. Raman, B. A. Remington, H. F. Robey, S. V. Weber, and K. Widmann, Phys. Rev. Lett. **112**, 185003 (2014).
[31] D. S. Clark, M. M. Marinak, C. R. Weber, D. C. Eder, S. W. Haan, B. A. Hammel, D. E. Hinkel, O. S. Jones, J. L. Milovich, P. K. Patel, H. F. Robey, J. D. Salmonson, S. M. Sepke, and C. A. Thomas, Phys. Plasmas **22**, 022703 (2015).
[32] C. R. Weber, T. Döppner, D. T. Casey, T. L. Bunn, L. C. Carlson, R. J. Dylla-Spears, B. J. Kozioziemski,

A. G. MacPhee, A. Nikroo, H. F. Robey, J. D. Sater, and V. A. Smalyuk, Phys. Rev. Lett. **117**, 075002 (2016); **117**, 159902 (2016);
[33] S. E. Bodner, D. G. Colombant, J. H. Gardner, R. H. Lehmberg, S. P. Obenschain, L. Phillips, A. J. Schmitt, J. D. Sethian, R. L. McCrory, W. Seka, C. P. Verdon, J. P. Knauer, B. B. Afeyan, and H. T. Powell, Phys. Plasmas **5**, 1901 (1998).
[34] V. A. Smalyuk, S. X. Hu, J. D. Hager, J. A. Delettrez, D. D. Meyerhofer, T. C. Sangster, and D. Shvarts, Phys. Rev. Lett. **103**, 105001 (2009).
[35] R. S. Craxton *et al.*, Phys. Plasmas **22**, 110501 (2015).
[36] S. E. Bodner, Phys. Rev. Lett. **33**, 761 (1974).
[37] M. H. Emery, J. H. Gardner, and S. E. Bodner, Phys. Rev. Lett. **57**, 703 (1986).
[38] R. Betti, R. L. McCrory, and C. P. Verdon, Phys. Rev. Lett. **71**, 3131 (1993).
[39] J. Sanz, Phys. Rev. Lett. **73**, 2700 (1994).
[40] J. D. Kilkenny, S. G. Glendinning, S. W. Haan, B. A. Hammel, J. D. Lindl, D. Munro, B. A. Remington, S. V. Weber, J. P. Knauer, and C. P. Verdon, Phys. Plasmas **1**, 1379 (1994).
[41] L. Masse, Phys. Rev. Lett. **98**, 245001 (2007).
[42] D. T. Casey, D. T. Woods, V. A. Smalyuk, O. A. Hurricane, V. Y. Glebov, C. Stoeckl, W. Theobald, R. Wallace, A. Nikroo, M. Schoff, C. Shuldberg, K. J. Wu, J. A. Frenje, O. L. Landen, B. A. Remington, and G. Glendinning, Phys. Rev. Lett. **114**, 205002 (2015).
[43] S. M. Gol'berg and A. L. Velikovich, Phys. Fluids B **5**, 1164 (1993).
[44] A. L. Velikovich, F. L. Cochran, and J. Davis, Phys. Rev. Lett. **77**, 853 (1996).
[45] J. H. Hammer, J. L. Eddleman, P. T. Springer, M. Tabak, A. Toor, K. L. Wong, G. B. Zimmerman, C. Deeney, R. Humphreys, T. J. Nash, T. W. L. Sanford, R. B. Spielman, and J. S. De Groot, Phys. Plasmas **3**, 2063 (1996).
[46] U. Shumlak and N. F. Roderick, Phys. Plasmas **5**, 2384 (1998).
[47] U. Shumlak, C. S. Adams, J. M. Blakely, B.-J. Chan, R. P. Golingo, S. D. Knecht, B. A. Nelson, R. J. Oberto, M. R. Sybouts, and G. V. Vogman, Nucl. Fusion **49**, 075039 (2009).
[48] S. P. Obenschain, D. G. Colombant, M. Karasik, C. J. Pawley, Y. Serlin, A. J. Schmitt, J. L. Weaver, J. H. Gardner, L. Phillips, Y. Aglitskiy, Y. Chan, J. P. Dahlburg, and M. Klapisch, Phys. Plasmas **9**, 2234 (2002).
[49] M. Karasik, J. L. Weaver, Y. Aglitskiy, J. Oh, and S. P. Obenschain, Phys. Rev. Lett. **114**, 085001 (2015).
[50] S. Fujioka, A. Sunahara, K. Nishihara, N. Ohnishi, T. Johzaki, H. Shiraga, K. Shigemori, M. Nakai, T. Ikegawa, M. Murakami, K. Nagai, T. Norimatsu, H. Azechi, and T. Yamanaka, Phys. Rev. Lett. **92**, 195001 (2004).
[51] S. X. Hu, G. Fiksel, V. N. Goncharov, S. Skupsky, D. D. Meyerhofer, and V. A. Smalyuk, Phys. Rev. Lett. **108**, 195003 (2012).
[52] G. Fiksel, S. X. Hu, V. A. Goncharov, D. D. Meyerhofer, T. C. Sangster, V. A. Smalyuk, B. Yaakobi, M. J. Bonino, and R. Jungquist, Phys. Plasmas **19**, 062704 (2012).
[53] A. G. MacPhee, J. L. Peterson, D. T. Casey, D. S. Clark, S. W. Haan, O. S. Jones, O. L. Landen, J. L. Milovich, H. F. Robey, and V. A. Smalyuk, Phys. Plasmas **22**, 080702 (2015).
[54] A. B. Bud'ko, M. A. Liberman, A. L. Velikovich, and F. S. Felber, Phys. Fluids B **2**, 1159 (1990).
[55] S. A. Sorokin and S. A. Chaikovskii, Plasma Phys. Rep. **19**, 444 (1993).
[56] S. A. Sorokin, Plasma Phys. Rep. **39**, 139 (2013).
[57] G. G. Zukakishvili, K. N. Mitrofanov, E. V. Grabovskiĭ, and G. M. Oleĭnik, Plasma Phys. Rep. **31**, 652 (2005).
[58] A. P. Orlov and B. G. Repin, Phys. Plasmas **23**, 092705 (2016).
[59] Axial velocity shear may actually be the primary stabilizing mechanism in twisted wire arrays, as described, e. g., in T. A. Golub, N. B. Volkov, R. B. Spielman, and N. A. Gondarenko, Appl. Phys. Lett. **74**, 3624 (1999); IEEE Trans. Plasma Sci. **28**, 1422 (2000); N. B. Volkov, T. A. Golub, R. B. Spielman, and N. A. Gondarenko, Laser Part. Beams **19**, 451 (2001).
[60] R. D. McBride and S. A. Slutz, Phys. Plasmas **22**, 052708 (2015).
[61] R. D. McBride *et al.*, Sandia National Laboratories Technical Report No. SAND2015-9860, 2015.
[62] See Supplemental Material at http://link.aps.org/supplemental/10.1103/PhysRevLett.117.205001 for the analytic growth rate formulas used in this Letter.
[63] We obtain Γ_{exact} by integrating explicitly the coupled ordinary differential equations (ODEs) for the linear MRTI perturbations without first applying the WKB ansatz that all perturbed quantities $\propto e^{i\omega t}$, where $\gamma_{mk} = \text{Im}(-\omega)$ for each set of mode numbers $(m, \vec{k})$. This exact solution is represented schematically as $\vec{\Psi}(t) = \hat{S}(t)\vec{\Psi}(0)$, where $\vec{\Psi}$ is a vector containing all of the independent scalar quantities describing the MRTI perturbations, and $\hat{S}(t)$ is the time-dependent (square) matrix describing the evolution of the coupled linear system. Denoting the ith eigenvalue of $\hat{S}(t)$ as $A_i(t)$, we define $\Gamma_{\text{exact}} \equiv \max[\ln|A_i(t)|]$ for $i \in \{1, 2, \ldots, n\}$, where n is the dimension of $\hat{S}$. In this case, we solve the coupled ODEs given by Eqs. (39b) and (40b) in Ref. [24], for which $\vec{\Psi} = [\xi_{\text{out}}, \xi_{\text{in}}, \dot{\xi}_{\text{out}}, \dot{\xi}_{\text{in}}]$, and thus $n = 4$. For more discussion, cf. Sec. II-C of Ref. [24].
[64] In words, Γ_{200} is the largest Γ_{mk} among all modes whose $\lambda(t_2) = 200\ \mu$m.
[65] Y. Y. Lau, J. C. Zier, I. M. Rittersdorf, M. R. Weis, and R. M. Gilgenbach, Phys. Rev. E **83**, 066405 (2011).
[66] D. V. Rose, D. R. Welch, T. P. Hughes, R. E. Clark, and W. A. Stygar, Phys. Rev. ST Accel. Beams **11**, 060401 (2008).
[67] C. A. Jennings, J. P. Chittenden, M. E. Cuneo, W. A. Stygar, D. J. Ampleford, E. M. Waisman, M. Jones, M. E. Savage, K. R. LeChien, and T. C. Wagoner, IEEE Trans. Plasma Sci. **38**, 529 (2010).
[68] E. A. Madrid, D. V. Rose, D. R. Welch, R. E. Clark, C. B. Mostrom, W. A. Stygar, M. E. Cuneo, M. R. Gomez, T. P. Hughes, T. D. Pointon, and D. B. Seidel, Phys. Rev. ST Accel. Beams **16**, 120401 (2013).
[69] R. D. McBride *et al.*, Phys. Plasmas **23**, 012705 (2016).
[70] S. A. Slutz, W. A. Stygar, M. R. Gomez, K. J. Peterson, A. B. Sefkow, D. B. Sinars, R. A. Vesey, E. M. Campbell, and R. Betti, Phys. Plasmas **23**, 022702 (2016).